VI International Conference on Computational Methods for Coupled Problems in Science and Engineering
COUPLED PROBLEMS 2015
B. Schrefler, E. Oñate and M. Papadrakakis (Eds)

AERODYNAMIC EXCITATION FORCES IN AIR CONDITIONERS WITH ROTATING FAN-MOTOR SYSTEM

T. SATO [*], S. NITA[†1], H. OTA[†2] AND K. NAGAHASHI[†2]

[*] Department of Mechanical Engineering, School of Engineering, Tokyo Denki University
5 Senju-Asahi-cho, Adachi-ku, Tokyo, 120-8551, Japan
e-mail: taichi@mail.dendai.ac.jp

[†1] Graduate School of Engineering, Tokyo Denki University
5 Senju-Asahi-cho, Adachi-ku, Tokyo, 120-8551, Japan

[†2] Hitachi Appliances Inc., Shimizu Air Conditioning Works
390 Muramatsu, Shimizu-ku, Shizuoka-shi, Shizuoka, 424-0926, Japan

Key words: Vibration, Noise, Aerodynamic Excitation Force, Outdoor unit, Air conditioner, CFD simulation.

Abstract. Aerodynamic pressure pulsation generated by rotating blades was measured using an experimental device consisting of fan blades, a motor, and pressure gauges. The motor was installed on a high-stiffness block via load cells and the motor reaction forces were measured by load cells. The aerodynamic pressure pulsation was also calculated using CFD simulation software, and based on those CFD results, motor reaction forces were also derived. Calculation results and experimental results were compared for both pressure pulsation and motor reaction forces and the calculations were found to agree well with experimental results.

1 INTRODUCTION

Many air conditioners use fan systems for heat exchange. Vibratory motion and noise in the air conditioner occur by the aerodynamic excitation forces generated by the rotating fan blades. Calculating these aerodynamic excitation forces is therefore a useful solution for reducing vibration and noise.

In this report, we investigate aerodynamic excitation forces in the outdoor unit of air conditioners (Fig. 1). Aerodynamic excitation forces in air conditioners having a fan-motor system can be divided into the following two types:

(1) aerodynamic pressure pulsation acting on the cabinet (the thin metal plate) of the air conditioner (referred to below as “aerodynamic pressure pulsation”), and

(2) reaction forces acting on the base of the motor as a result of aerodynamic pressure pulsation (referred to below as “motor reaction forces”).

In terms of prior work, Ota et al. measured the aerodynamic pressure pulsation and researched techniques for predicting structural vibration caused by the pressure pulsation [1]. Sato et al. discussed the relationship between aerodynamic pressure pulsation and motor reaction force experimentally [2]. Furukawa et al. simulated the vertical flow in a propeller

fan using large eddy simulation [3]. Watanabe et al. discussed the aerodynamic and noise characteristics of a centrifugal fan [4].

In the study reported here, we measured the aerodynamic pressure pulsation of the rotating blades using an experimental device consisting of fan blades, a motor, pressure gauges, and load cells. The motor, which has four feet at its base, was installed on a high-stiffness block via load cells. Fan blades were attached to the motor axis by screwing them on through bosses. A measurement board was installed for receiving aerodynamic pressure pulsation, which was measured using a pressure sensor attached to the measurement board.

We also calculated the aerodynamic pressure pulsation on the measurement board and fan blades using CFD simulation software, and based on those CFD results, we also derived motor reaction forces. We compared calculation results and experimental results for both pressure pulsation and motor reaction forces and found that the calculations agreed well with the results obtained by experiment.

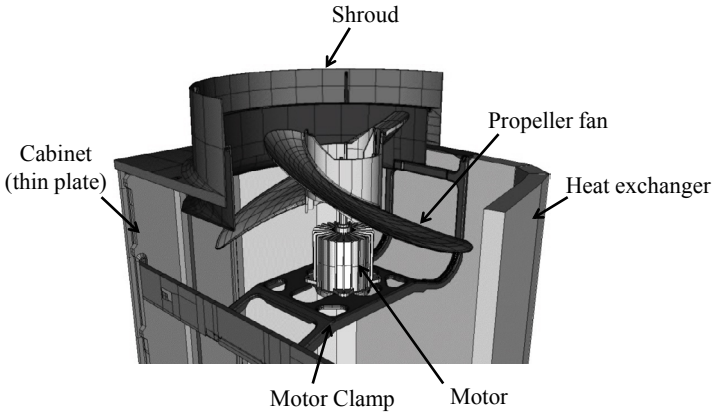

Figure 1: Outdoor unit of air conditioners

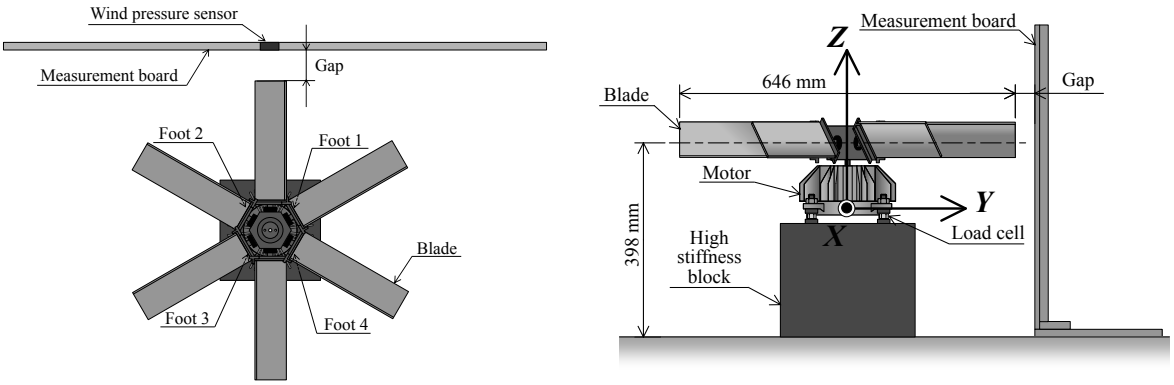

(a) Top view (b) Side view

Figure 2: Experimental setup

2 EXPERIMENTAL MEASUREMENTS AND CALCULATION OF AERODYNAMIC PRESSURE PULSATION

A top view and side view of the experimental setup are shown in Figs. 2 (a) and (b), respectively. The motor has four feet at its base. The right-front foot facing the measurement board is called “foot 1” while the other feet are numbered as “foot 2,” “foot 3,” and “foot 4” in a counterclockwise direction.

The motor is installed on a high-stiffness block via load cells. Six fan blades are screwed on to the motor axis at equal intervals through bosses, and each fan blade is installed with a 60-degree tilt from the horizontal. The direction of this tilt is the direction of upward aerodynamic flow generated by the fan.

The measurement board shown in Fig. 2 receives the aerodynamic pressure pulsation of the rotating fan blades. It corresponds to one of the thin metal plates making up the cabinet of an outdoor air conditioning unit. Here, the distance of closest approach between the measurement board and the tip of a fan blade is called the “gap.” In this experiment, we fix this gap to 10 mm and the rotating speed of the motor to 225 rpm.

A wind pressure sensor is installed on the measurement board at the position shown in Fig. 3. It is installed at a height of 398 mm corresponding to the heightwise center of the fan blades. Since the fan blades pass in front of the measurement board from right to left, the coordinate system of the measurement board is arranged accordingly with numerical signs running from minus to plus. The point corresponding to the closest approach of the fan blades (the center of the measurement board in the horizontal direction) is taken to be the origin of this coordinate system.

The results of measuring the aerodynamic pressure pulsation on the measurement board for the three measuring points shown in Fig. 3 are shown in Fig. 4 (solid line). These experimental results represent average values over time and therefore exclude the random components characteristic of aerodynamic excitation forces. We also performed a computational fluid dynamics (CFD) analysis using the standard k-ε model in fluid flow analysis software PHOENICS developed by CHAM Limited. The calculation results of this analysis (dashed line) are shown in the figure superposed on the experimental results. It can be seen that the calculations represent the experimental results well in terms of magnitude and waveform.

The results of performing a frequency analysis on the results obtained for aerodynamic pressure pulsation in Fig. 4 are shown in Fig. 5. A major peak can be observed at 22.5 Hz for both experimental results and calculations. This frequency, called the blade passing frequency (BPF), is given by the product of the rotating speed of the motor and the number of fan blades. Calculations agree well with experimental results for both the BFF (22.5 Hz) component and its higher frequency components.

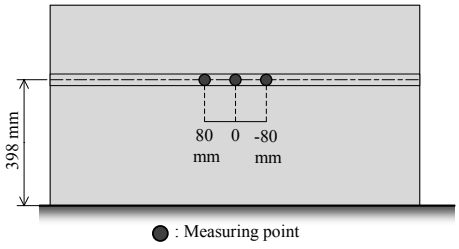

Figure 3: Three measuring points on measurement board

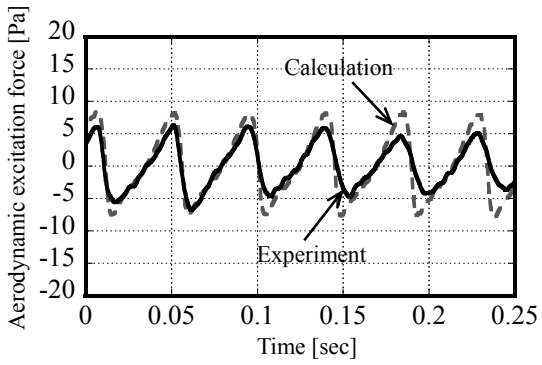

(a) -80mm

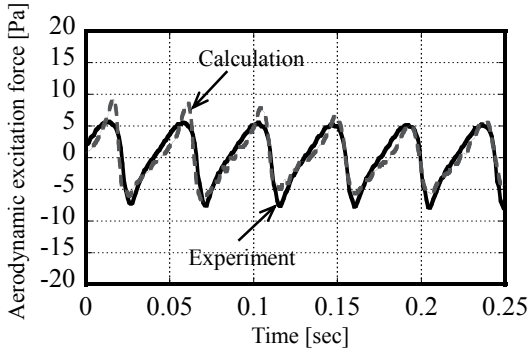

(b) 0mm

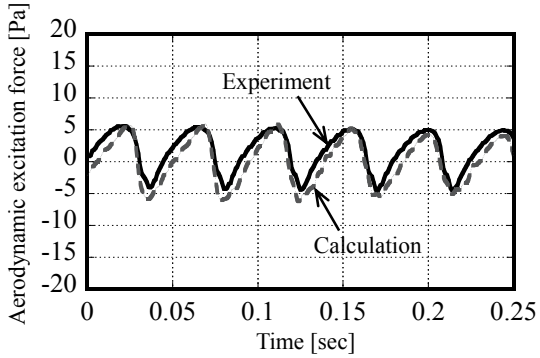

(c) 80mm

Figure 4: Time history response of aerodynamic pressure pulsation

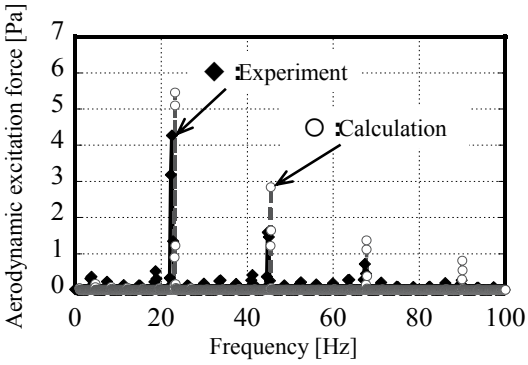

(a) -80mm

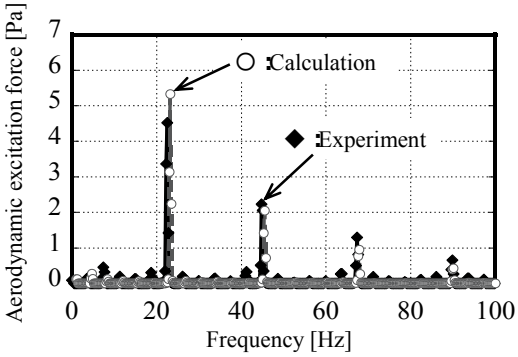

(b) 0mm

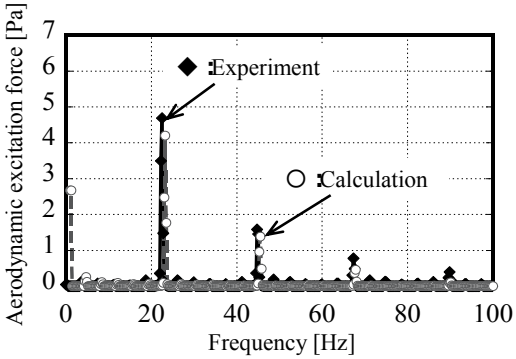

(c) 80mm

Figure 5: FFT results of aerodynamic pressure pulsation

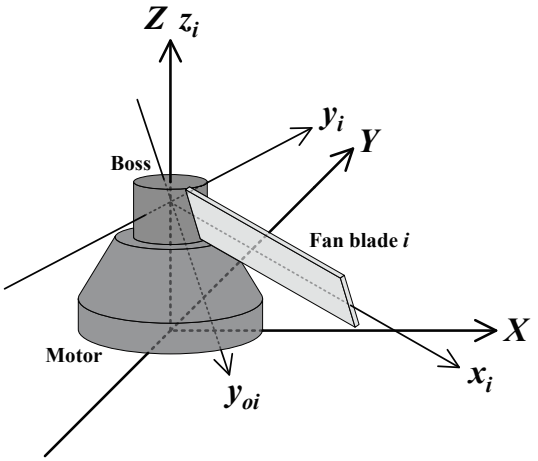

Figure 6: Coordinate system

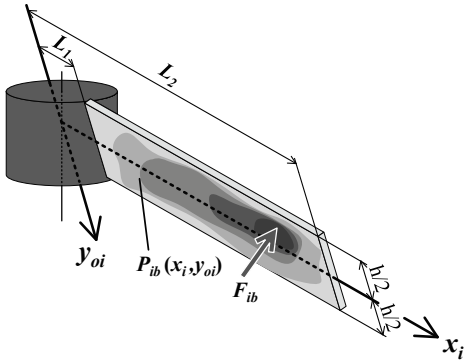

Figure 7: Pressure distribution and concentrated load

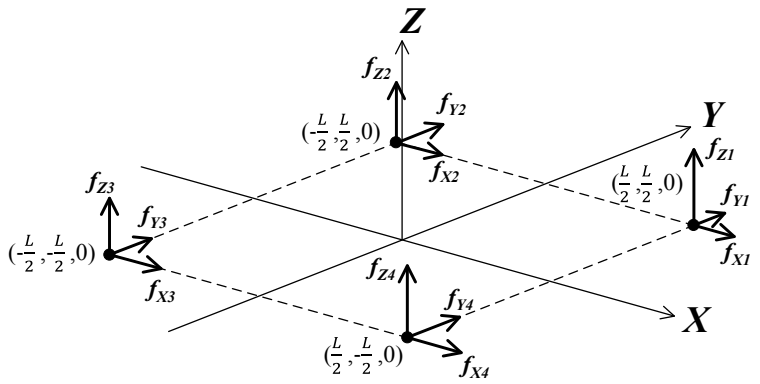

Figure 8: Force received at the motor's foot-support points

3 CALCULATION PROCEDURE AND CALCULATION/EXPERIMENTAL RESULTS OF MOTOR REACTION FORCES

We also calculated the pressure acting on the fan-blade surface in the CFD analysis described above and used those results to calculate the motor reaction forces by the procedure described below.

As shown in Fig. 6, the fan-motor system is installed in the *X*-*Y*-*Z* coordinate system of Fig. 2 fixed in space. The four motor feet lie on the *X*-*Y* plane. The origin of this *X*-*Y*-*Z* coordinate system is the point where the plane formed by the motor feet (*X*-*Y* plane) intersects the motor's axis.

The measurement board shown in Fig. 4 constitutes the plane that intersects the *Y* axis at the *Y* coordinate equal to "fan radius + gap."

In addition, the x_i-y_i-z_i coordinate system is fixed to the *i*th fan blade (*i*=1–*N*, where *N* is the number of fan blades; *N*=6 in this study), which means that it rotates with the blade. As shown in Fig. 6, the x_i-y_i plane runs parallel to the *X*-*Y* plane, but the wind-receiving surface

of fan blade i tilted with respect to the horizontal plane is separately specified as the x_i - y_{oi} plane.

Next, as shown in Fig. 7, pressure $P_{ia}(x_i, y_{oi})$ and $P_{ib}(x_i, y_{oi})$ acting on the surface of the ith fan blade can be replaced by concentrated loads F_{ia} (acting point (x_{ia}, y_{ia}, z_{ia})) and F_{ib} (acting point (x_{ib}, y_{ib}, z_{ib})) applied to the fan blade. Here, suffixes a and b denote the front surface facing the direction of movement (pressure surface) and the rear surface (suction surface), respectively. We point out here that the surface acted on by pressure $P_{ia}(x_i, y_{oi})$ is on the side of the blade not shown in the figure, so $P_{ia}(x_i, y_{oi})$ and F_{ia} do not explicitly appear in the figure.

In addition, we convert concentrated loads F_{ia} and F_{ib} to component forces (F_{Xia}, F_{Yia}, F_{Zia}) and (F_{Xib}, F_{Yib}, F_{Zib}), respectively, corresponding to the axes in the X-Y-Z coordinate system, and likewise convert concentrated-load acting points (x_{ia}, y_{ia}, z_{ia}) and (x_{ib}, y_{ib}, z_{ib}) to coordinates (X_{ia}, Y_{ia}, Z_{ia}) and (X_{ib}, Y_{ib}, Z_{ib}), respectively, in the X-Y-Z coordinate system.

As a result, we can replace the pressure acting on the fan-blade surface with the load acting at the origin of the X-Y-Z coordinate system and the moments about each axis in the X-Y-Z coordinate system as given by Eqs. (1) and (2).

$$\begin{pmatrix} F_X \\ F_Y \\ F_Z \end{pmatrix} = \sum_{i=1}^{N} \left\{ \begin{pmatrix} F_{Xia} \\ F_{Yia} \\ F_{Zia} \end{pmatrix} + \begin{pmatrix} F_{Xib} \\ F_{Yib} \\ F_{Zib} \end{pmatrix} \right\} \tag{1}$$

$$\begin{pmatrix} M_X \\ M_Y \\ M_Z \end{pmatrix} = \sum_{i=1}^{N} \left\{ \begin{pmatrix} X_{ia} \\ Y_{ia} \\ Z_{ia} \end{pmatrix} \times \begin{pmatrix} F_{Xia} \\ F_{Yia} \\ F_{Zia} \end{pmatrix} + \begin{pmatrix} X_{ib} \\ Y_{ib} \\ Z_{ib} \end{pmatrix} \times \begin{pmatrix} F_{Xib} \\ F_{Yib} \\ F_{Zib} \end{pmatrix} \right\} \tag{2}$$

Now, if we denote the force received at the motor's foot-support points from foot 1 to foot 4 as shown in Fig. 8, Eqs. (3) and (4) hold based on the balance of forces and balance of moments, respectively, on the motor.

$$\begin{pmatrix} F_X \\ F_Y \\ F_Z \end{pmatrix} = \begin{pmatrix} -f_{X1} - f_{X2} - f_{X3} - f_{X4} \\ -f_{Y1} - f_{Y2} - f_{Y3} - f_{Y4} \\ -f_{Z1} - f_{Z2} - f_{Z3} - f_{Z4} \end{pmatrix} \tag{3}$$

$$\begin{pmatrix} M_X \\ M_Y \\ M_Z \end{pmatrix} = \frac{L}{2} \begin{pmatrix} -f_{Z1} - f_{Z2} + f_{Z3} + f_{Z4} \\ f_{Z1} - f_{Z2} - f_{Z3} + f_{Z4} \\ (f_{X1} - f_{Y1}) + (f_{X2} + f_{Y2}) - (f_{X3} - f_{Y3}) - (f_{X4} + f_{Y4}) \end{pmatrix} \tag{4}$$

Here, L denotes the interval from one foot to the other.

A fan-motor system in an outdoor air conditioning unit is generally attached to the thin-plate support structure. It therefore becomes necessary to apply an out-of-plane load when such a system is causing the thin-plate support structure to vibrate. In other words, F_Z and M_X, and M_Y in Eqs. (3) and (4) take on particular importance at this time.

Assuming that the stiffness of the motor is sufficiently high compared with the stiffness of the structure supporting the motor, and using the geometrical relationship of the four motor feet positioned on the same plane, motor reaction forces $f_{Z1} - f_{Z4}$ can be given by Eq. (5) using F_Z and M_X, and M_Y determined from Eqs. (3) and (4).

$$
\begin{aligned}
f_{z1} &= -\frac{F_z}{4} - \frac{M_X - M_Y}{2L} \\
f_{z2} &= -\frac{F_z}{4} - \frac{M_X + M_Y}{2L} \\
f_{z3} &= -\frac{F_z}{4} + \frac{M_X - M_Y}{2L} \\
f_{z4} &= -\frac{F_z}{4} + \frac{M_X + M_Y}{2L}
\end{aligned}
\tag{5}
$$

Based on the flow described above, we calculated the motor reaction forces. We found that the main frequency component of motor reaction forces was also the same BPF component (22.5 Hz) as that for aerodynamic pressure pulsation described in the previous section.

On the basis of this result, we decided to compare the results obtained by calculations with those by experiment for the BPF component of motor reaction forces for all four feet. The resulting temporal waveforms for the BPF component are shown in Fig. 9. It can be seen that calculation results reproduce well the experimental results in terms of magnitude and phase difference for the motor feet. This result demonstrates that motor reaction forces can be calculated with sufficient accuracy by the sequence of calculations presented in this report.

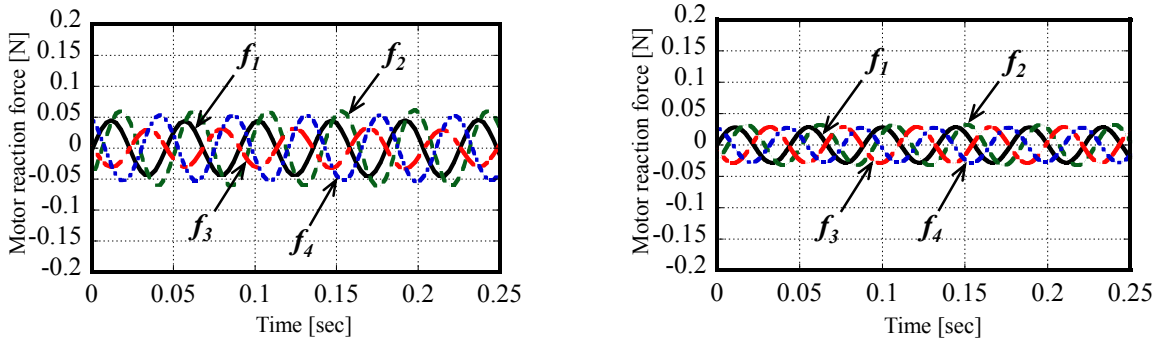

(a) Calculation (b) Experiment

Figure 9: BPF component of motor reaction forces

4 CONCLUSIONS

- In this paper, we investigated aerodynamic pressure pulsation and motor reaction forces as aerodynamic excitation forces generated by a rotating fan-motor system. We showed that pressure pulsation on a measurement board as determined by experiment could be represented well by the results of CFD analysis. We also

determined the pressure pulsation on the fan-blade surface by CFD analysis and used that result to also derive a formula for calculating the motor reaction forces. We found that the results of calculating motor reaction forces with that formula agreed well with experimental results, which demonstrated that motor reaction forces could be calculated with sufficient accuracy.

REFERENCES

[1] Ota et al., Direct measurement of aerodynamic excitation force generated by rotating-blade fan, Noise Control Eng. J. 57(4), July-Aug 2009, pp. 310-317, 2009.
[2] Sato et al., Aerodynamic excitation force generated by rotating-blade fan and its reaction force, MIPE2012, pp. 40-42, 2012.
[3] Furukawa, et al., Analysis of unsteady pressure field in a propeller fan using large eddy simulation, Proceedings of JSCFD, B07-2, 1999 (in Japanese).
[4] Watanabe et al., Prediction of aerodynamic noise of fans, Trans. Jpn. Soc. Mech. Eng., Vol. 66, No. 642, pp. 453-459, 2000 (in Japanese).